Linear and Nonlinear Description of Drift Instabilities in a High Beta Plasma

A. Y. Aydemir, H. L. Berk, V. Mirnov,[a]
O. P. Pogutse,[b] and M. N. Rosenbluth
Institute for Fusion Studies
The University of Texas at Austin
Austin, Texas 78712

December 1986

[a] Permanent Address: Institute of Nuclear Physics
Novosibirsk, USSR.
[b] Permanent Address: Kurchatov Institute, Moscow, USSR.

Linear and Nonlinear Description of Drift Instabilities
in a High Beta Plasma

A. Y. Aydemir, H. L. Berk, V. Mirnov,[a]

O. P. Pogutse,[b] *and M. N. Rosenbluth*

Institute for Fusion Studies

The University of Texas at Austin

Austin, Texas 78712

Abstract

A nonlinear system of equations is derived for drift waves in a high beta plasma ($\beta \gg 1$). The magnetic field pressure is taken small compared to the particle pressure. Pressure balance is established by having a uniform particle pressure with the density and temperature gradients in opposite directions. The primary purpose of the magnetic field is to inhibit radial heat flux. This is the principle of such plasma fusion systems as the wall sustained multiple mirror, compressed liner, and magnetic-insulated inertial fusion, where the heat is contained over a relatively short radial scale length and a long axial scale length. The nonlinear equations for the mathematical model contain drift instabilities which give rise to radial heat and particle fluxes that can enhance the losses expected from classical collisional effects. The linear and nonlinear evolution of the model is studied here.

[a] Permanent Address: Institute of Nuclear Physics, Novosibirsk, USSR.
[b] Permanent Address: Kurchatov Institute, Moscow, USSR.

I. Introduction

In most controlled fusion concepts, one attempts to use the pressure of magnetic fields to confine hot plasma. However, there exist some concepts[1,2,3] where cold plasma pressure is used to confine hotter plasma. In such a system the plasma is cold and dense on the outside, and hotter but less dense on the inside. The pressure equilibrium is characterized by nT = constant in space, where n is the density, and T the temperature. The role of magnetic field is not to supply confining pressure, but only to provide thermal insulation across field lines. Thus, such a system can be short radially (perpendicular to the magnetic field) where thermal conduction is relatively low, and long axially where conduction is larger.

One of the problems of such confinement concepts is the likelihood of instabilities arising because of density and temperature gradients. Linear drift wave instabilities have been reported for such systems.[4,5,6] It is the purpose of this paper to study linear high beta drift wave theory and to make a preliminary nonlinear investigation of the effect of such drift wave instabilities. In our nonlinear model the instability does cause a deterioration of thermal confinement, but at some parameter regimes close enough to marginal stability, the saturation level may be low enough to maintain good thermal insulation.

In Sec. II, we develop a linear theory for high beta drift wave instabilities based on kinetic theory. In Sec. III, we show how fluid equations can be posed that qualitatively reproduces the linear instability predictions of kinetic theory. To investigate the nonlinear behavior, we consider a simplified fluid model that has a simple equation of state based on the ion population having a conserved magnetic moment that depends only on **r**. The linear theory of the simpler model is qualitatively similar to that of the original fluid model, and we expect qualitatively similar nonlinear behavior. In Sec. IV, we present numerical results. Close to marginal stability these results show quasilinear saturation, with appreciable temperature gradients remaining. However, more unstable regimes cause flattening of most of the temperature profile. In Sec. V, conclusions are presented.

II. Linear Theory

We consider a system where

$$\beta = \frac{8\pi p_0}{B^2} \gg 1. \tag{1}$$

Then, in equilibrium, the perpendicular pressure balance equation is

$$p_i + p_e + \frac{B^2}{8\pi} \simeq p_i + p_e \equiv n_0(x)\left[T_e(x) + T_i(x)\right] = p_0, \tag{2}$$

and p_0 is independent of space. For simplicity we also take $T_e(x)/T_i(x)$ to be space independent. The equilibrium density and temperature profiles are shown in Fig. 1. The magnetic field is present only to inhibit heat conduction which arises if $\omega_{cj}/\nu_j \gg 1$, where ω_{cj} is the cyclotron frequency of species j, and ν_j is its collision frequency. We use the kinetic equation in the low-frequency eikonal approximation. The perturbed field amplitudes are taken as,

$$\mathbf{E} = -\boldsymbol{\nabla}\phi - \frac{1}{c}\frac{\partial \mathbf{A}}{\partial t},$$

$$\mathbf{B}_1 = \boldsymbol{\nabla} \times \mathbf{A},$$

$$\mathbf{A} = \frac{\mathbf{B}_0 \times \boldsymbol{\nabla}\Lambda}{B_0} + \frac{A_\parallel \mathbf{B}}{B_0}$$

are their spatial variation is taken as $\exp(i\mathbf{k}\cdot\mathbf{r})$. The linearized form of the kinetic equation for the perturbed distribution f_{1j}, with the equilibrium distribution Maxwellian (i.e., $f_{0j} = \left(2\pi T_j/m_j\right)^{1/2}\exp\left(-E/T_j\right)$ with E the particle energy, and T_j and m_j the temperature and mass of species j), is[7]

$$-i\left(\omega - \omega_{Bj} - k_\parallel v_\parallel\right)\left(f_{1j} + \frac{q_j}{T_j}\phi f_{0j} - \frac{\boldsymbol{\nabla}\Lambda\cdot\boldsymbol{\nabla}f_{0j}}{B_0}\right)$$

$$= -i\frac{q_j}{T_j}\left[\omega - \omega_{*j}\left(\frac{5}{2} - \frac{m_j v^2}{2T_j}\right)\right]f_{0j}\exp\left[\frac{i\mathbf{k}\times\mathbf{v}\cdot\mathbf{b}}{\omega_{cj}}\right] \tag{3}$$

$$\cdot\left[\left(\phi - \frac{v_\parallel A_\parallel}{c}\right)J_0\left(\frac{k_\perp v_\perp}{\omega_{cj}}\right) + \frac{2\mu B_\parallel\omega_{cj}}{k_\perp v_\perp q_j}J_1\left(\frac{k_\perp v_\perp}{\omega_{cj}}\right)\right],$$

where $B_\parallel = -k_\perp^2\Lambda$ is the perturbed parallel magnetic field, $\mathbf{b} = \mathbf{B}_0/|B_0|$ and $\omega_{Bj} = cv_\perp^2\mathbf{k}\times\boldsymbol{\nabla}B_0/2q_jB_0 \equiv \text{grad } B$ drift. Note that in Ref. 7 the term $\boldsymbol{\nabla}\Lambda\cdot\boldsymbol{\nabla}f_{0j}/B_0$ does not appear as it is of higher order in the eikonal approximation. However, keeping this term

3

in linear theory does not add additional complexity to the analysis. Also, if we define $\mathbf{k} \times \mathbf{v} \cdot \mathbf{b} = k_\perp v_\perp \sin\psi$, we have

$$\exp\left[\frac{i\mathbf{k} \times \mathbf{v} \cdot \mathbf{b}}{\omega_{cj}}\right] = \sum_n J_n\left(\frac{k_\perp v}{\omega_{cj}}\right)\exp(in\psi).$$

We have also used

$$\frac{1}{n_0}\frac{\partial n_0}{\partial x} = -\frac{1}{T_{0j}}\frac{\partial T_{0j}}{\partial x}, \qquad \omega_{*j} = \frac{ck_y T_{0j}}{q_j B_0 n_0}\frac{\partial n_0}{\partial x}.$$

We define $\omega_* \equiv \omega_{*e}$, and $\tau = T_i/T_e$. We assume $(T_i/m_i)^{1/2} \ll \omega/k_\parallel \ll (T_e/m_e)^{1/2}$ as the drift instabilities are likely to occur in this parameter range. [Analysis when $\omega/k_\parallel v_e \gg 1$ is given in Ref. 6.] Under this assumption, the parallel current due to ions is negligible compared to the electron current, since the appropriate moment of Eq. (3) yields $j_{\parallel i} \sim (k_\parallel v_i/\omega)^2 j_{\parallel e}$. We also assume $k_\parallel \ll k_\perp$. The field equations for ϕ, $A_\parallel$, $B_\parallel$ are determined from the first three moment equations, which in our limit take on the form,

$$q_i n_{i1} + q_e n_{e1} = 0 + O\left(k_\perp^2 \lambda_D^2\right) \quad \text{(quasi} - \text{neutrality)}, \tag{4}$$

$$j_{\parallel e1} = 0 + O\left(j_{\parallel i1}/j_{\parallel e1}\right) + O\left(k_\perp^2 L_n^2/\beta\right) \quad \text{(parallel Ampere's law)}, \tag{5}$$

$$\mathbf{k} \cdot (\mathbf{p}_{\perp e1} + \mathbf{p}_{\perp i1}) \cdot \mathbf{k} = 0 + O(1/\beta) \quad \text{(pressure balance)}, \tag{6}$$

where $\lambda_D \equiv$ Debye length, and $L_n^{-1} = d\ln n_0/dx$, and $\mathbf{p}_{\perp j}$ is a pressure tensor defined below. The densities and parallel current are evaluated from the moments $\int d^3v f_{1j} = n_{1j}$ and $q_e \int d^3v v_\parallel f_{1e} = j_{\parallel e}$. We need to be somewhat careful in the definition of ion pressure, which is a tensor with finite Larmor radius (FLR) effects. Assuming the perturbed ion pressure is diagonal, although not scalar (which is confirmed by explicitly showing $\int d^3v \mathbf{k}_\perp \cdot \mathbf{v}_\perp \mathbf{k} \times \mathbf{v} \cdot \mathbf{b} f_{0j} = 0$), we need to evaluate

$$i\mathbf{k} \cdot \mathbf{p}_{\perp i_1} \cdot \mathbf{k} = m_i \sum_j \int d^3v \left(\mathbf{k}_\perp \cdot \mathbf{v}\right)^2 f_{1j}. \tag{7}$$

One can observe that if the first charge moment is taken of Eq. (3), the use of Eqs. (4)–(6) will allow a degenerate relationship to be satisfied to lowest order in Larmor radius for any choice of field amplitudes. This enables us to obtain the effects of the

4

finite Larmor radius terms relatively simply. We multiply Eq. (3) by q_j, integrate over velocity space and sum over species. We then find that on the left-hand side the terms containing f_{1j} nearly vanish by the use of the linearized forms of Eqs. (4)–(6). The only term that survives on the left-hand side is from the ion finite Larmor radius effects on the perturbed pressure. Using Eq. (7), we have

$$\sum_j \int q_j \omega_{Bj} f_1 d^3 v \equiv \frac{c}{B_0^2} k_y \frac{\partial B_0}{\partial x} \sum_j \int d^3 v \, m_j \frac{v_\perp^2}{2} f_{1j}$$

$$= m_i \frac{c}{B_0^2} \frac{\partial B_0}{\partial x} k_y \int d^3 v \left(\frac{v^2}{2} - \left(\hat{\mathbf{k}} \cdot \mathbf{v} \right)^2 \right) f_{1i}, \tag{8}$$

where we have taken only zeroth order electron Larmor radius effects and $\hat{\mathbf{k}} = \mathbf{k}/|k|$.

Now solving Eq. (3) for f_{1i}, to second order in Larmor radius terms, yields

$$f_{1i} = \frac{q_i \left[\omega + \tau \omega_* \left(\frac{5}{2} - \frac{mv_i^2}{2T} \right) \right]}{T_i \left(\omega - \omega_{Bi} \right)} f_{0i} \left(1 + \frac{k_\parallel v_i}{\omega - \omega_{Bi}} \right)$$

$$\cdot \left[1 - i \frac{k_\perp v_\perp}{\omega_{ci}} \sin \psi - \frac{1}{2} \left(\frac{k_\perp v_\perp}{\omega_{ci}} \right)^2 \sin^2 \psi + \frac{i}{8} \left(\frac{k_\perp v_\perp}{\omega_{ci}} \right)^3 \sin^3 \psi \right]$$

$$\cdot \left[\left(1 - \frac{k_\perp^2 v_\perp^2}{4\omega_{ci}^2} \right) \left(\phi - \frac{v_\parallel A_\parallel}{c} \right) + \frac{v_\perp^2}{2} \frac{B_\parallel}{B_0 q_i} \left(1 - \frac{k_\perp^2 v_\perp^2}{8\omega_{ci}^2} \right) \right]$$

$$- \frac{q_i}{T_i} \phi \tau f_{0i} + \frac{\nabla \Lambda \cdot \nabla f_{vi}}{B} + \mathcal{O} \left[\left(\frac{k_\perp v_\perp}{\omega_{ci}} \right)^4 \right] + \mathcal{O} \left[\left(\frac{k_\parallel v_i}{\omega} \right)^2 \right], \tag{9}$$

Then substituting Eq. (9) into the left-hand side of Eq. (8), yields

$$\sum_j \int q_j \omega_{Bj} f_{1j} d^3 v = \bar{\omega}_B \frac{m}{16 T_i} \int_0^\infty dv_\perp v_\perp^3 \frac{\left[\omega - \omega_{*i} \left(2 - \frac{mv_\perp^2}{T_i} \right) \right]}{(\omega - \omega_{Bi})} \exp\left(-m_i v_\perp^2 / T_i \right)$$

$$\times \frac{k_\perp^2 v_\perp^2}{\omega_{ci}^2} \left[\phi + \frac{B_\parallel v_\perp^2}{2 q_i B_0} \right] \tag{10}$$

with $\bar{\omega}_B = \frac{c k_y T_i}{q_i B_0^2} \frac{\partial B_0}{\partial x}$, and note that only finite Larmor radius terms remain on the right-hand side.

We also find that the zero-order Larmor radius terms on the right-hand side of Eq. (8) (i.e., to the extent $J_0 \left(\frac{k_\perp v_\perp}{\omega_{cj}} \right) = 1$ and $\omega_{cj} J_1 \left(\frac{k_\perp v_\perp}{\omega_{cj}} \right) \Big/ k_\perp v_\perp = 1/2$) automatically vanish,

and to have the right-hand side nonzero we need to use $J_0(x) - 1 = -x^2/4 + \mathcal{O}(x^4)$, $J_1(x) - x/2 = -x^3/16 + \mathcal{O}(x^5)$. As a result the charge density moment of Eq. (3) has the form

$$\bar{\omega}_B \frac{(k_\perp a_i)^2}{4} \int_0^\infty dx \exp(-x) \frac{x^2 \left[\omega + \tau\omega_*(2 - x)\right]\exp(-x)}{\omega - \bar{\omega}_B x} \cdot \left[\phi + \frac{B_\parallel}{B_0 q_i}\frac{T_i}{m_i}x\right] =$$

$$-(k_\perp a_i)^2 \left[\phi + \frac{3}{2}\left(1 - \frac{\omega_*\tau}{\omega}\right)\frac{T_i B_\parallel}{q_i B}\right], \tag{11}$$

where

$$a_i^2 = \frac{T_i}{m_i \omega_{ci}^2}, \qquad \bar{\omega}_B = \left(\frac{ck_y T_i}{q_i B_0^2}\right)\left(\frac{dB_0}{dx}\right).$$

We now use the solution of Eq. (3) to evaluate Eqs. (5) and (6). We find to lowest order in Larmor radius

$$j_{\parallel e} = q_e \int d^3v\, v_\parallel f_e$$

$$= -n_{e0}\omega q_e \left[\frac{Q_L}{B_0 k_\parallel} + iq_e \frac{(\omega - \omega_*)E_\parallel}{\omega T_e k_\parallel^2}\right]\left(1 + O\left(\frac{\omega}{k_\parallel v_e}\right)\right) = 0 \tag{12}$$

$$\hat{\mathbf{k}}_\perp \cdot (\mathbf{p}_{\perp e} + \mathbf{p}_{\perp i}) \cdot \hat{\mathbf{k}}_\perp = \sum_j \int d^3v\, m_j f_{1j} v_\perp^2/2 = q_e n_{e0} \frac{E_\parallel}{ik_\parallel}\left[1 + O\left(\frac{\omega}{k_\parallel v_e}\right)\right]$$

$$- q_i n_{i0} \frac{E_\parallel}{ik_\parallel} \int_0^\infty \frac{dx \exp(-x)x}{\Omega - x}\left[x + \frac{\omega_*\tau}{\bar{\omega}_B}(2 - x)\right]\left[1 + O\left(\frac{k_\parallel v_i}{\omega}\right)\right]$$

$$+ \frac{Q_L}{B} n_{i0} T_i \int_0^\infty \frac{dx\, x^2 \exp(-x)}{\Omega - x}\left[\Omega + \frac{\omega_*\tau}{\bar{\omega}_B}(2 - x)\right]\left[1 + O\left(\frac{k_\parallel v_i}{\omega}\right)\right] = 0, \tag{13}$$

where $\Omega = \omega/\bar{\omega}_B$, $Q_L = B_\parallel + k_y\left(dB_0/dx\right)\left(A_\parallel/k_\parallel B_0\right)$ (the perturbed Lagrangian magnetic field), and $E_\parallel = -ik_\parallel\phi + \frac{i\omega}{c}A_\parallel$ (parallel electric field).

One observes that Eqs. (12) and (13) only depend on two field amplitudes, $E_\parallel$ and Q_L, and hence describe a closed system, independent of a third amplitude. Thus, these two equations, which describe arbitrary excitations, are independent of the finite Larmor radius condition given in Eq. (11). If desired, the third polarization amplitude can be obtained from Eq. (4). Even more important, we note that there is one special non-trivial

6

degree of freedom where $Q_L = E_\parallel = 0$, but with the field amplitudes nonzero. This arises if

$$B_\parallel = -\frac{k_y}{k_\parallel B_0}\frac{\partial B_0}{\partial x}A_\parallel, \qquad \phi = \frac{\omega A_\parallel}{k_\parallel c}. \tag{14}$$

Substituting this relation into Eq. (11) allows for an additional mode of oscillation. The dispersion relation is found to be

$$\omega^2 - \omega\bar{\omega}_B + \omega_* \tau \bar{\omega}_B = 0. \tag{15}$$

This dispersion relation is the usual magnetohydrodynamic (MHD)-like finite Larmor radius result in the limit in which the ion pressure gradient vanishes.[8] In the general FLR theory the term $\tau\bar{\omega}_B\omega_*$ is due to a fourth moment of the distribution function. Thus, stability is guaranteed if $\bar{\omega}_B/\omega_* < 0$, while if it is greater than zero, stability requires

$$\frac{1}{\alpha} \equiv \frac{\omega_*\tau}{\bar{\omega}_B} = \frac{\partial\ln T_i}{\partial\ln B_0} < \frac{1}{4}. \tag{16}$$

We now solve Eqs. (12) and (13) when $E_\parallel$ and Q_L are finite. From Eq. (12) and the equilibrium quasineutrality condition, we find

$$iq_i\frac{E_\parallel}{k_\parallel} = \frac{Q_L T_e \omega}{B_0\left(\omega - \omega_*\right)}.$$

Then substitution into Eq. (13) yields the dispersion relation

$$D(\Omega) \equiv 1 + \int_0^\infty \frac{dx\exp(-x)}{\Omega - x}\left[x^2 + \frac{x}{\alpha}(2-x) + x^2\left(\tau - \frac{1}{\alpha\Omega}\right)\left(\Omega + \frac{(2-x)}{\alpha}\right)\right] = 0, \tag{17}$$

where $\Omega = \omega/\bar{\omega}_B$.

To determine the marginal stability conditions of Eq. (17), we first rewrite the dispersion relation in the form

$$D(\Omega) = G(\Omega) + H(\Omega)\int_0^\infty dx\frac{x^2\exp(-x)}{\Omega - x} = 0, \tag{18}$$

where

$$G(\Omega) = 1 + \frac{2}{\Omega\alpha} + \frac{2}{\alpha}\left(\tau - \frac{1}{\Omega\alpha}\right)$$

$$H(\Omega) = \frac{2}{\alpha\Omega} - \frac{\Omega}{\alpha}\left(\tau - \frac{1}{\Omega\alpha}\right) + 1 - \frac{1}{\alpha} + \left(\tau - \frac{1}{\Omega\alpha}\right)\left(\Omega + \frac{2}{\alpha}\right).$$

7

If at marginal stability $\Omega > 0$, then the real and imaginary parts of Eq. (18) must vanish separately, which implies that both $H(\Omega) = 0$ (from the imaginary part vanishing) and hence, $G(\Omega) = 0$. We then find that at marginal stability,

$$\frac{\partial \ln B_0}{\partial \ln T_i} \equiv \alpha = \frac{1}{2(1 + \tau)} \equiv \alpha_{cr1}$$

$$\Omega = \frac{4(1 + \tau)}{1 + 2\tau} \equiv \Omega_{cr1}. \tag{19}$$

One can readily show that stability requires $\alpha > \alpha_{cr1}$.

If at marginal stability $\Omega < 0$, then marginal stability requires

$$D(\Omega, \alpha) = 0 \qquad \text{and} \qquad \frac{\partial D(\Omega, \alpha)}{\partial \Omega} = 0. \tag{20}$$

In general, the marginal condition must be found numerically for the roots $\alpha = \alpha_{cr2}$, $\Omega = \Omega_{cr2}$ for a given τ. In Fig. 2 we graph τ and Ω_{cr2} vs. $-\alpha_{cr2} = -\frac{d \ln B}{d \ln T_i}$. These solutions can be understood analytically at $\alpha = 0$ and near $\alpha = 1$. At $\alpha = 0$, the dispersion relation is

$$\omega^2(1 + 2\tau) - 2\omega_*\omega\tau(1 + \tau) + 2\tau^2\omega_*^2 = 0, \tag{21}$$

with the root,

$$\omega = \frac{\omega_*\tau}{(1 + 2\tau)}\left[1 + \tau \pm \left(\tau^2 - 1 - 2\tau\right)^{1/2}\right].$$

This root has been obtained by Mikhailovsky[4] for $\tau = 1$. Stability requires $\tau > 1 + \sqrt{2}$, and the important case of $\tau = 1$ is always unstable. If $\tau > 1 + \sqrt{2}$, one can readily show that if α is small and positive, $\Omega > 0$ and ion Landau damping destabilizes the lower frequency solution, while if α is small and negative, $\Omega < 0$ and there is no Landau damping. Stability will then exist as long as $-\alpha$ is less than $-\alpha_{cr2}$. For $-\alpha > -\alpha_{cr2}$, instability is present. For large $|\alpha|$ one can show the mode frequency is given by

$$\Omega = \frac{\Omega_*^2\tau^2}{1 + \tau}\left[1 - \frac{2\pi i}{(1 + \tau)\alpha}\right], \tag{22}$$

so that if $-\alpha \gg 1$ we have instability, and if $\alpha \gg 1$ we have stability.

One can solve Eqs. (18) and (20) as $\tau \to \infty$. Assuming $\Omega^2\tau \approx \mathcal{O}(1)$ and $y \approx -1$, the dispersion relation becomes

$$D(\Omega) = \Omega^2\tau\left(1 - \frac{1}{\alpha}\right) + \Omega\tau\left(1 + \frac{1}{\alpha}\right) - \frac{1}{\alpha^2} + 2\frac{\Omega^2\tau}{\alpha}\left(\ln\left(-\frac{1}{\Omega}\right) - \gamma\right) \tag{23}$$

8

with $\gamma = 0.635$ being Euler's constant. Setting $\alpha_{cr2} = -1 + \delta\alpha_{cr2}$ leads to the rough marginal stability condition

$$\frac{\delta\alpha_{cr2}^2}{\ln\left[\delta\alpha_{cr2}\tau/2\right]} = \frac{8}{\tau}. \tag{24}$$

Combining the results of these analyses we conclude that if $\tau = T_i/T_e < 1 + \sqrt{2}$ the stability criteria to zero-order FLR and finite-FLR modes are respectively

$$\frac{\partial \ln B_0}{\partial \ln T_i} > \frac{1}{2(1+\tau)}, \tag{25}$$

and

$$\frac{\partial \ln B_0}{\partial \ln T_i} < 0 \qquad \text{or} \qquad \frac{\partial \ln B_0}{\partial \ln T_i} > 4. \tag{26}$$

If $\tau > 1 + \sqrt{2}$, an additional stability band appears for the zero-order FLR modes given by

$$\alpha_{cr2}(\tau) < \frac{\partial \ln B_0}{\partial \ln T_i} < 0, \tag{27}$$

where α_{cr2} is negative and is given in Fig. 2. It is significant this stability band is compatible with stability criteria to the FLR mode given in Eq. (26). Note that we have not considered stabilization or destabilization by parallel Landau damping.

9

III. Nonlinear Equations

We have constructed a model set of equations to describe the nonlinear properties of the zero-order FLR mode.

To model the ion motion we note that $k_\parallel = 0$ and the flow velocity is

$$\mathbf{v}_\perp = c\frac{\mathbf{E} \times \mathbf{B}}{B^2} - \frac{c}{n|e|B^2}\left(\nabla p_i \times \mathbf{B}\right). \tag{28}$$

If we substitute this form into the continuity equation, we find after using $\frac{1}{c}\frac{\partial B}{\partial t} = -\mathbf{z}\cdot\nabla\times\mathbf{E}$ and some additional straight forward manipulation,

$$\frac{d}{dt}\ln(N) + (\mathbf{v}_B \cdot \nabla)\ln(\sigma) = 0, \tag{29}$$

where $N = n_i/B$, $\sigma = T_i/B$, and

$$\frac{d}{dt} = \frac{\partial}{\partial t} + (\mathbf{v}_\phi + \mathbf{v}_B + \mathbf{v}_\lambda)\cdot\nabla. \tag{30}$$

The drift velocities appearing above are given by:

$$\mathbf{v}_\phi = c\frac{\mathbf{z}\times\nabla\phi}{B}, \qquad \mathbf{v}_B = \frac{\sigma}{|e|}\mathbf{z}\times\nabla\ln(B), \qquad \mathbf{v}_\lambda = -\frac{1}{B}\nabla\frac{\partial\Lambda}{\partial t}. \tag{31}$$

To close the system we choose an ion model distribution with a single magnetic moment at each point of space. This model allows for an exact fluid description of the ions. With magnetic moment conservation, the equation of motion is simply

$$\frac{d\sigma}{dt} = 0, \tag{32}$$

with $\sigma = T_i/B$. For the electron density, we have noted that the linear response is close to a Maxwell-Boltzman response. Hence we model the nonlinear electron density as,

$$n_e = n_0 \exp\left(\frac{|e|\phi}{T_e}\right). \tag{33}$$

The final equation is the pressure balance equation, which at high beta has the form

$$n_i T_i + n_e T_e = p_0, \tag{34}$$

where we somewhat arbitrarily set $T_e = T_0(x)$, with n_0, and T_0 determined by Eq. (36) below. The final set of nonlinear equations then has the form

$$\frac{d}{dt}\ln(N) + (\mathbf{v}_B \cdot \nabla)\ln(\sigma) = 0,$$

$$\frac{d}{dt}\sigma = 0,$$

$$\frac{d}{dt} = \frac{\partial}{\partial t} + (\mathbf{v}_\phi + \mathbf{v}_\lambda + \mathbf{v}_B) \cdot \nabla,$$

$$\frac{|e|\phi}{T_0} = \ln\left(N\frac{B}{n_0}\right),$$

$$B^2 N\sigma + \frac{BNT_0}{\tau} = p_0, \tag{35}$$

and

$$\text{a)} \quad T_0 = \int T_i dy \Big/ \int dy, \qquad \text{b)} \quad n_0 = \frac{p_0}{T_0(1+\tau)}. \tag{36}$$

Equation (33) is of course only a crude approximation to the electron response which is to a considerable extent determined by 3-dimensional flow along field lines, beyond the scope of this paper. However, using the moment equations, we estimate $B_r/B_0 \sim \frac{1}{3}k_\parallel\xi$, or the field flutter amplitude $\Delta r \sim \frac{1}{3}\xi$ with $\xi \sim (k_\perp\phi/\omega B)$, the displacement in the plane. In this connection we may estimate the stochastic field thermal transport

$$\chi_e = v_e D_{\text{mag}} \approx \frac{1}{10}k_\parallel v_e \xi^2.$$

Since $k_\parallel v_e \geq \omega$, depending on the dominant longitudinal structure of the modes, these neglected processes may be important and our results are a lower limit on transport.

Equation (36a), together with Eq. (33), is equivalent to the condition $\partial\langle\phi\rangle/\partial x \sim 0$, imposed by the constraint that there is no mechanism present for developing macroscopic fluid velocities (rotation in the cylindrical case).

For simplicity, our simulations neglect the $\mathbf{v}_\lambda$ term in Eq. (35). Including $\mathbf{v}_\lambda$ in a few check runs did not alter the results.

To examine the linear stability of our nonlinear model we have for $\beta \to \infty$,

$$n = n_0(x) + n_1,$$

11

$$T_i = T_0(x) + T_1,$$

$$B = B_0(x) + B_\parallel,$$

$$T_e = T_0(x)/\tau. \tag{37}$$

The pressure balance equation and the linearized Boltzman law then give

$$\frac{\tau}{(1+\tau)}\frac{T_1}{T_0} = -\frac{n_1}{n_0} = -\frac{\phi|e|\tau}{T_0}. \tag{38}$$

The linearization of the form (dg/dt), with $g = g_0 + g_1$, is

$$\frac{dg}{dt} \rightarrow -i(\omega - \omega_B)g_1 - \frac{ick_y T_i}{|e|B}\left[\frac{n_1}{\tau n} + \frac{B_1}{B}\right]\frac{dg_0}{dx}, \tag{39}$$

with $\omega_B = \left(ck_y T_0/|e|B_0^2\right)(dB_0/dx)$. Using Eq. (39) and the equations in (35) yield

$$[(1+1/\tau)\omega_B + \omega_* - \omega]\frac{n_1}{n_0} + \omega\frac{B_\parallel}{B_0} + \omega_B\frac{T_1}{T_0} = 0, \tag{40}$$

$$(\omega_B - \omega)\frac{T_1}{T_0} + (\omega - \tau\omega_*)\frac{B_\parallel}{B_0} + \frac{n_1}{n_0}\left(\frac{\omega_B}{\tau} - \omega_*\right) = 0. \tag{41}$$

With $(n_1/n_0) = -\tau T_1/(1+\tau)$, the dispersion relation becomes

$$\omega^2(2+\tau) - \omega\left[\omega_*(1 + \tau + \tau^2) + \bar\omega_B\tau\right] - \omega_*^2\tau^2 = 0. \tag{42}$$

The instability regime is then found to be

$$-(1 + \tau + \tau^2) - 2\tau(2+\tau)^{1/2} < \frac{d\ln B_0}{d\ln T_i} < -(1 + \tau + \tau^2) + 2\tau(2+\tau)^{1/2}. \tag{43}$$

An alternate fluid model, which includes heat flux from finite Larmor radius effects, gives a description of instability quantitatively closer to the kinetic description, especially when $|d\ln B_0/d\ln T_i| \ll 1$. The heat flow equation for ions can be written as

$$\frac{\partial p_\perp}{\partial t} + \mathbf{v}_i \cdot \nabla p_\perp + \gamma_0 \nabla \cdot \mathbf{v}_i + \nabla \cdot q = 0, \tag{44}$$

where γ_0 is the adiabatic index, taken here as 2 here and q the heat flux. If we neglect collisional effects and parallel heat flow, the off-diagonal heat flux $\mathbf{q}_T$ remains, and is given by[9]

$$\mathbf{q}_T = \frac{\gamma_0}{\gamma_0 - 1}\frac{cp_i}{q_i B}\hat{\mathbf{z}} \times \nabla T_i. \tag{45}$$

12

If we use Eq. (31), we find that including the flux causes the evolution equation in Eq. (35) to be modified to

$$\frac{d\sigma}{dt} + \frac{\mathbf{v}_B \cdot \nabla(\sigma^2 N)}{\sigma N} = 0. \tag{46}$$

This equation is not totally consistent, but it appears to produce favorable properties when its consequences are compared to the linearized kinetic analysis. When we linearize this equation, it leads to the following form that replaces Eq. (41)

$$(3\omega_B - \omega)\frac{T_1}{T_{i0}} + \frac{B_\parallel}{B_0}(\omega - 2\omega_*\tau) + \frac{n_1}{n}\left(\frac{2\omega_B}{\tau} - \omega_*\right) = 0. \tag{41$'$}$$

Equations (40), (41$'$) and the relation $n_1/n_0 = -\tau T_1/(1+\tau)T_0$ then leads to the dispersion relation

$$\omega^2(1 + 2\tau) - \omega\left[2\omega_*\tau(1+\tau) + \omega_B(1+3\tau)\right] + 2\omega_*^2\tau^2 = 0. \tag{47}$$

For $\frac{d\ln B_0}{d\ln T_0} = 0$, this is the same dispersion as obtained in kinetic theory for a Maxwellian plasma. The instability band predicted by Eq. (47) is

$$-\frac{2}{1+3\tau}\left[1 + \tau + (2+4\tau)^{1/2}\right] < \frac{d\ln B_0}{d\ln T_0} < -\frac{2}{1+3\tau}\left[1 + \tau - (2+4\tau)^{1/2}\right].$$

At marginal stability the frequency is given by

$$\Omega_{flc} \equiv \frac{\omega}{\omega_B} = \frac{1}{\alpha(1+2\tau)}\left[1 + \tau + \alpha(1+3\tau)/2\right]. \tag{48}$$

One notes that the stability parameters predicted by one side of this band

$$\frac{d\ln B_0}{d\ln T_0} = -\frac{2}{1+3\tau}\left[1 + \tau - (2+4\tau)^{1/2}\right] \equiv \alpha_{flc} \tag{49}$$

tracks closely with the marginal stability predictions of kinetic theory. For $\tau > 1 + \sqrt{2}$ the correlation is shown comparing in Fig. 2 the dotted curves, which is for the heat flux model with the solid curves, which is the result of kinetic theory. For $\tau < 1 + \sqrt{2}$, we note from Eqs. (19) and (49) that the ratio of the predicted $d\ln B_0/d\ln T_0$ values is given by Table I.

Most of our nonlinear numerical investigations ignored the heat term in Eq. (46). However, as the linear theory, where the heat term is included, seems to track well with the kinetic theory with thermal effects, we have also implemented a nonlinear code that includes this heat term. The results are briefly described in the next section.

13

IV. Numerical Results

Equations (35) and (36) are numerically integrated in a two-dimensional slab geometry with periodic boundary conditions assuming $T_e = T_i$. For reasons of convenience and numerical accuracy, a hybrid scheme is used. The quantity $N = n_i/B$ is advanced in time using standard second-order accurate finite-difference schemes. However, convection of the magnetic moment, σ, using such schemes tends to introduce unwanted numerical diffusion, especially when the equilibrium gradients are large, and the modes are highly unstable. In order to minimize such numerical effects, a particle-in-cell method[10] is adopted for advancing σ. Particles with an initially uniform spatial distribution are assigned magnetic moments corresponding to the local value of $\sigma = T_i/B$. They are then convected with the local drift velocity. σ is interpolated onto the finite-difference mesh from the particle positions using standard techniques when needed. Typically, a 64 by 64 mesh with eight particles per cell are used in nonlinear calculations.

a) Linear Calculations

The dispersion relation, Eq. (42), and the instability window of Eq. (43) are checked numerically using a linearized version of Eqs. (35) and (36). In practice this linearization is accomplished by numerically filtering out the unwanted wavelengths from various quantities at each time-step. The results of this linear code agree quite well with Eqs. (42) and (43). Figure 3 shows the growth rate as a function of the wavenumber k_y for a uniform magnetic field case, $\omega_B/\omega_* = 0$. As we have introduced filtering at short wavelengths, the numerically calculated growth rates decrease as k_y approaches the largest wavenumber allowed in the system, $k_{y\,max}/2\pi = 32$ in this case. In Fig. 4, we plot the growth rate for various values of the instability parameter, $\alpha \equiv (d \ln B_0/d \ln T_0)$. Except for the limit of $\omega_B/\omega_* \rightarrow -6$, which implies large field gradients even for moderate temperature gradients, again the computational results and theory agree quite well. Note that the growth rate has a maximum at $\alpha = \omega_B/\omega_* = -3$. The reduction in growth rates beyond that point, and the eventual stabilization at $\alpha = -6.46$ can be attributed to the increasing grad-B drift as the field becomes more diamagnetic. The stabilizing influence of a large $\mathbf{v}_B$ can be seen in the first two equations of (35) by balancing $(\partial/\partial t)$ and $(\mathbf{v}_B \cdot \nabla)$ terms, which

14

leads to stable oscillations at $\omega = \omega_B/3$.

b) Nonlinear Results

As stated earlier, the primary purpose of the magnetic field in the high-β devices under consideration here is to inhibit radial heat flux. For this purpose, it is desirable to have magnetic field act only as a thermal barrier. However, instability can cause deterioration of this insulation. In this nonlinear study we hope to obtain some insight on whether thermal insulation can be attained. In order to assess the effects of nonlinear evolution of these instabilities on transport, various initial conditions corresponding to different values of the instability parameter $\omega_B/\omega_* = d\ln B_0/d\ln T_0$ are examined. In all cases, the density and temperature profiles of Fig. 1 are used. The initial magnetic field is given by $B_0(x) = T_0(x)^\alpha$, where $\alpha = \omega_B/\omega_*$.

The nonlinear results will be discussed in terms of two typical cases. In the first one, the magnetic field is uniform ($\alpha = 0$), which is unstable but not far from the marginal stability point at $\alpha = 0.46$. The instability is observed to saturate through quasilinear modification of the equilibrium: the density and temperature gradients are reduced, while the magnetic field becomes larger in the high temperature region (Figs. 5, 6). The overall effect is to increase α to approximately 0.5, at which point the instability shuts off. The modification of the temperature profile associated with the quasilinear saturation is not very severe; the temperature peak decreases by 15%, but otherwise particle and energy confinement is maintained. Note that the change of gradient introduced into the magnetic field will reduce the effectiveness of the thermal barrier, since the field in the cold plasma region is decreased.

The second case with $\alpha = -1.2$ has an initially radially increasing magnetic field. However, the drift instabilities have a larger growth rate for $\alpha = -1.2$, and their nonlinear evolution has a more pronounced effect on confinement. The initial density and temperature profiles are the same as in the $\alpha = 0$ case (Fig. 1); the initial magnetic field profile is shown in Fig. 7. The temperature and the magnetic field at saturation are shown in Figs. 8, 9, respectively. Note that the y-averaged temperature profile, $\langle T \rangle_y (x)$, has essentially become flat, resulting in loss of confinement. More importantly, the gradients

15

for $\langle T \rangle_y$ and $\langle B \rangle_y$ are no longer in opposite directions. The hot and cold plasma regions have exchanged places (compare Figs. 1b, and 8b), and the instability parameter α has become positive. This is in contrast to the previous case which reached quasilinear saturation ($\alpha \geq 0.46$) essentially through modification of the magnetic field while approximately maintaining the initial temperature gradient.

The deterioration of confinement increases as α becomes more negative, which can be attributed to the increased level of turbulence as the magnetic field is excluded from the interior in the equilibrium. Figure 10 shows $\delta B/B$ at saturation as a function of α, where $\delta B/B$ is defined as

$$\frac{\delta B}{B} = \left[\left\langle (B - B_0)^2 \right\rangle \right]^{1/2} \bigg/ \langle B_0 \rangle . \qquad (50)$$

The brackets denote surface averages, and B_0 is the initial field. Note that a factor of two increase in $\delta B/B$ in going from $\alpha = 0$ to $\alpha = -1.2$ shown in Fig. 10 somewhat underestimates the increase in the turbulence level. For $\alpha = 0$, Eq. (50) essentially measures the coherent modification of the initially uniform magnetic field, not the true level of turbulence.

A better indication of the loss of confinement is shown in Fig. 11, where a measure of the residual temperature gradient in the saturated state is plotted. Near the marginal stability point $\alpha = 0.46$, the temperature gradient rapidly decreases with α. For $\alpha \leq -0.5$, the loss of confinement becomes catastrophic, as discussed above for the $\alpha = -1.2$ case, in the sense that the temperature profile basically becomes flat, with the residual gradient indicating a radial exchange of hot and cold plasma regions.

Qualitative differences in confinement between $\alpha = 0$, and $\alpha = -1.2$ cases can also be seen in Fig. 12. Figure 12a shows the position of a "test-particle" (one of the particles used in σ advection) at various points in time for $\alpha = 0$; in Fig. 12b, the positions of the same particle are given for $\alpha = -1.2$. In the $\alpha = 0$ case, the radial excursions of the particle are relatively small, while it drifts mainly in the y-direction. In Fig. 12b however, the drift orbit of the particle indicates no radial confinement at all; it is not lost from the system only because of the imposed periodic boundary conditions.

Nonlinear calculations near the second marginal stability point at $\alpha = -6.4$ are difficult to perform, as the large value of $|\alpha|$ requires using a very fine mesh, and therefore an

16

expensive calculation. Furthermore, in an extensive run with $\alpha = -6.0$, we found that the diffusion of the field reduces α and thus pushes the plasma to the unstable regime. Thus, rather than saturating quasilinearly, the plasma becomes more unstable, again leading to flattening of the profiles. However, in this case the numerical accuracy of our integration is suspect, and we are not positive whether our nonlinear instability is physical or just numerical.

Nonlinear calculations above have ignored the heat flux term (Eq. (45)) in the evolution of $\sigma = T_i/B$. As noted in the previous section, using the more complete heat flow equation for ions, Eq. (46), gives closer agreement with the kinetic theory results of Sec. II. Thus, for comparison, we have also performed calculations using Eq. (46) for the time evolution of σ, rather than the simple convection loss, $d\sigma/dt = 0$.

For $\tau = T_i/T_e = 1$, the dispersion relation, Eq. (47), predicts the instability band

$$-2.23 < \frac{d\ln B_0}{d\ln T_0} < 0.23.$$

Our linear calculations exhibit stability for $\alpha = d\ln B_0/d\ln T_0 > 0.23$, and $\alpha < -2.23$, in agreement with the linear theory. Moreover, now near both of the marginal points, the instability achieves quasilinear saturation without serious effects on confinement. This contrasts with the previously described simulation where we achieved quasilinear saturation only near the positive marginal point. Away from the marginal points ($\alpha \simeq -1$), however, confinement degradation is severe. There results are summarized in Fig. 13, which shows the residual temperature gradient after saturation as a function of $(-\alpha)$.

V. Summary and Conclusions

Drift instabilities have been examined for high-β systems where the magnetic field pressure is negligible compared to particle pressure. The primary purpose of the magnetic field, B_0, is to inhibit radial heat flux from the region of large temperature, T_0.

A linear theory based on kinetic theory predicts that two types of drift waves are excited in the limit $\omega/k_\parallel v_e \ll 1$, with v_e the electron thermal velocity. One type, with the perturbed parallel electric field, $E_\parallel$, finite, can be calculated with zero-Larmor radius theory, while the second mode, which has $E_\parallel = 0$, requires finite Larmor radius terms to obtain an appropriate description. If $\tau \equiv T_i/T_e < 1 + \sqrt{2}$, the stability criteria for the two modes are:

(a) zero-Larmor radius mode

$$\alpha \equiv \frac{\partial \ln B_0}{\partial \ln T_i} > \frac{1}{2(1+\tau)};$$

(b) finite-Larmor radius mode

$$\alpha = \frac{\partial \ln B_0}{\partial \ln T_i} < 0 \qquad \text{or} \qquad \frac{\partial \ln B_0}{\partial \ln T_i} > 4.$$

These criteria make it difficult to find a stable operating range since $\alpha < 0$ is unstable to the zero-Larmor radius mode and achieving $\alpha > 4$, where both modes would be stable, means a rapid radial fall-off of the magnetic field, a condition that may be technologically difficult. In fact, one usually envisages systems where the magnetic field is larger on the outside than the inside.[1] If $\tau > 1 + \sqrt{2}$, it appears possible to find a parameter range simultaneously stable to the two drift wave modes. If $\alpha < 0$, the finite-Larmor radius mode is stable, and there is a band

$$-|\alpha_{cr2}| < \alpha < 0$$

which is stable to the zero-Larmor radius mode, where $-\alpha_{cr2}$ is given in Fig. 2 as a function of τ. Perhaps this regime is optimum for stable operation of magnetically thermally insulated systems.

A fluid set of equations was formulated to describe the nonlinear evolution of the zero-Larmor radius mode. If collisionless heat flow is included, the linearized fluid equations

18

has quite similar stability properties as the kinetic theory, especially if $\left|\frac{d \ln B_0}{d \ln T_i}\right| \ll 1$. Two self-consistent nonlinear set of equations has also been formulated and in this work we have studied numerically the time evolution of these equations. In one model there is zero heat flow, which is exact for an ion distribution that is a delta function in the magnetic moment. The other model includes ion heat flow, based on a somewhat arbitrary truncation procedure, whose stability boundaries are qualitatively similar to the kinetic theory.

In the numerical simulation where we choose $T_e = T_i$, we find that an initially unstable equilibrium profile close to marginal stability relaxes to a stable profile. However, for initial profiles significantly different from the marginal one, we find that most of the thermal insulation is lost, and the final temperature difference between the inside and the outside becomes quite small. For example, for the zero heat flow model with $\alpha = -1.2$, we show that thermal insulation is lost in one drift time of the longest wavelength. Similar results arise with the heat flow model. For a constant profile, this implies a loss rate, $\tau_L^{-1} \approx q_i \frac{c}{B_0 x} \frac{\partial T_i}{\partial x}$ where $k_y L_n \sim 1$ with L_n the macroscopic scale length. This loss is similar to the Bohm diffusion rate, even perhaps an order of magnitude faster if one takes into account the numerical factor of $1/16$ in Bohm diffusion. Thus, the simulation indicates that systems with profiles with $\alpha = \frac{\partial \ln B_0}{\partial \ln T_i} \approx -1$ (which one expects from modeling in simple magnetic field configurations) and with $T_e/T_i \approx 1$ have poor confinement.

Better containment may be obtained if profiles with $\alpha > 0$ can be formed or if plasmas with $T_e/T_i < 1$ can be established. The simulation indicated that if an equilibrium is unstable but not too far from the marginal stability profile of the zero Larmor radius mode, the system relaxes to the marginally stable profile. For the zero-Larmor radius mode the marginally stable value of $\alpha_{cr} = \frac{\partial \ln B_0}{\partial \ln T_i}$ is moderate, e.g., in the kinetic theory $\alpha_{cr} = 1/4$. However, stability to the finite-Larmor radius mode requires a more severe condition, which is $\frac{\partial \ln B_0}{\partial \ln T_i} > 4$. Hence, if the nonlinear properties of the finite-Larmor radius mode is similar to the zero-Larmor radius mode, very rapidly decreasing magnetic field profiles are needed to maintain stability.

We have already pointed out that if $T_e/T_i < 1/(1+\sqrt{2})$, one can find negative values of $\partial \ln B_0/\partial \ln T_i$ that are stable to both types of drift waves. In such a region, radial thermal insulation should be maintained. A lower electron temperature than ion temperatures may

in fact be physically easy to achieve, as parallel thermal conductivity losses pass primarily through the electron channel.

Acknowledgements

References

1. G. E. Vekshtejn, V. V. Mirnov, D. D. Ryutov, P. Z. Chebotaev, in *Proceedings of the Sixth Conference on Plasma Physics and Controlled Nuclear Fusion Research*, Berchtesgaden, (International Atomic Energy Agency, Vienna, 1977), Vol. III, p. 535.

2. D. L. Book, A. L. Cooper, R. Ford, K. A. Gerber, D. A. Hammer, D. J. Jenkins, A. E. Robson, P. J. Turchi, in *Proceedings of the Sixth Conference on Plasma Physics and Controlled Nuclear Fusion Research*, Berchtesgaden, (International Atomic Energy Agency, Vienna, 1977), Vol. III, p. 507.

3. A. Hasegawa, H. Daido, M. Fujita, K. Mima, M. Murakami, S. Nakai, K. Nishihara, K. Terai, C. Yamanaka, Phys. Rev. Letters **56**, 139 (1986).

4. A. B. Mikhailovskii, Soviet Physics, Doklady **15**, 471 (1970).

5. A. El-Nadi, M. N. Rosenbluth, Phys. Fluids **16**, 2036 (1973).

6. Y. A. Dreizin, E. P. Sokolov, Fizika Plazmy **12**, 184 (1986) [Trans: Soviet J. Plasma Physics **12**, 107 (1986)].

7. T. M. Antonsen, Jr., B. Lane, Phys. Fluids **23**, 1205 (1980).

8. L. D. Pearlstein and H. A. Krall, Phys. Fluids **9**, 2231 (1966).

9. S. I. Braginski, in **Reviews of Plasma Physics** (Consultants Bureau, New York, 1965), edited by M. A. Leontovich, Vol. I, p. 205.

10. R. L Morse, in **Methods in Computational Physics** (Academic Press, New York, 1970), edited by Berni Alder, Vol. 9, p. 213.

Table I

τ	α_{cr1}	α_{flc}	$\alpha_{flc}/\alpha_{cr1}$
2.00	.167	.046	0.28
1.50	.200	.119	0.59
1.00	.250	.225	0.90
0.75	.286	.30	1.05
0.50	.333	.40	1.20
0.25	.400	.55	1.37
0	.500	.83	1.66

Table I: List of critical values for stability of $\alpha = d\ln B_0/d\ln T_i$ from kinetic theory (α_{cr1}) and fluid theory (α_{flc}) with heat flow for various value of $\tau = T_i/T_e$.

Figure Captions

1. Equilibrium profiles used in nonlinear calculations: a) Density, b) temperature. For numerical reasons, the cold plasma region is chosen to be at the center. Since periodic boundary conditions are employed, the physics of the problem is not altered by this choice.

2. Solid curves are the marginal stability parameter $-\alpha_{cr2}$ and the marginal frequency $-\Omega_{cr2}$ as function of ion to electron temperature ratio τ. Also included in dotted curves is the prediction of the stability parameters of the fluid model with heat flow, Ω_{flc} and α_{flc}, given in Eqs. (48) and (49). The stable region is on the lower right part of the graph.

3. The growth rate as a function of the mode number for a uniform magnetic field case.

4. The growth rate as a function of the instability parameter $\alpha = \omega_B/\omega_*$.

5. Temperature at saturation for $\alpha = 0$. a) Contours in the $x - y$ plane with the maximum and minimum values of temperature indicated below the graph, b) y-averaged temperature profile.

6. Magnetic field at saturation for $\alpha = 0$. a) Contours in the $x - y$ plane with the maximum and minimum values of magnetic field indicated below the graph, b) y-averaged field profile. Initially field is uniform for this case.

7. Initial magnetic field profile for $\alpha = -1.2$: a) Contours in the $x - y$ plane with the maximum and minimum values of magnetic field indicated below the graph, b) $B_0^{'}(x)$.

8. Temperature at saturation for $\alpha = -1.2$: a) Contours with the maximum and minimum values of temperature indicated below the graph, b) y-averaged profile.

9. Magnetic field at saturation for $\alpha = -1.2$: a) Contours with the maximum and minimum values of magnetic field indicated below the graph, b) y-averaged profile.

10. $\delta B/B$ as a function of the instability parameter $\alpha = \omega_B/\omega_*$.

11. $\Delta T/\Delta T_0$ as a function of the instability parameter α, where $\Delta T \equiv \langle T \rangle_{y\,\max} - \langle T \rangle_{y\,\min}$. $\langle T \rangle_y$ denotes y-average of T, and T_0 is the initial temperature.

12. Test particle orbits: a) $\alpha = 0.$, b) $\alpha = -1.2$. The location of the particle at $t = 0$ is circled.

13. $\Delta T/\Delta T_0$ as a function of the instability parameter α for the nonlinear model with heat flux. See caption of Figure 11 for definition of ΔT and ΔT_0.
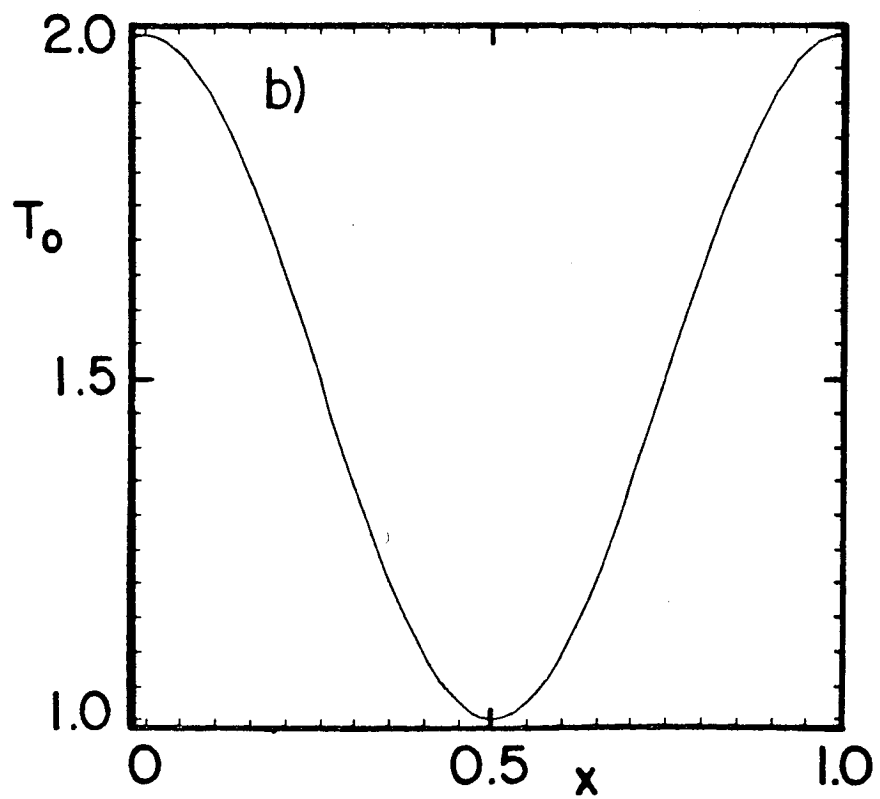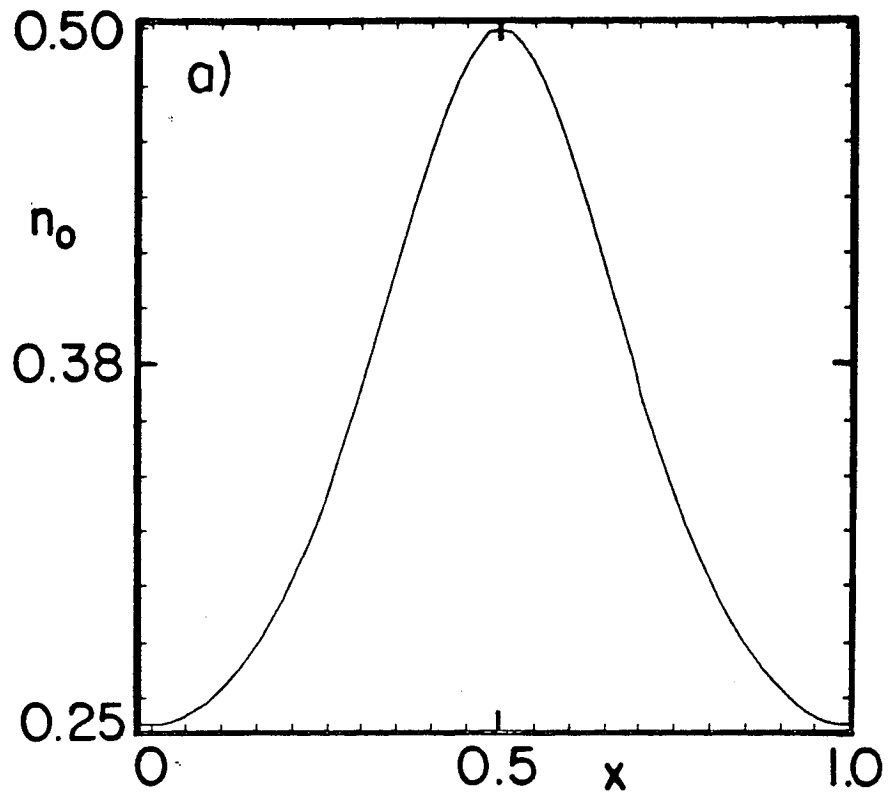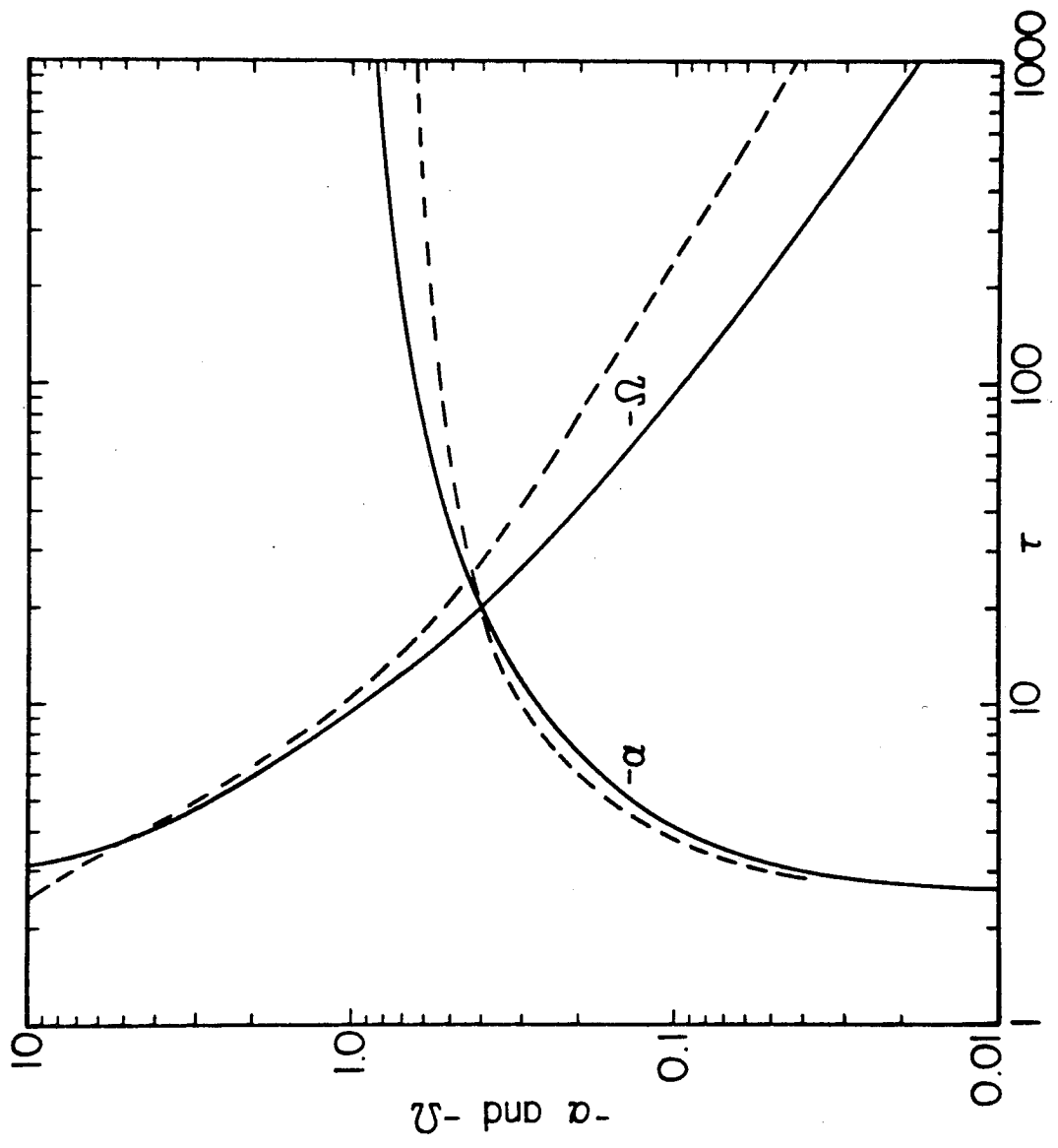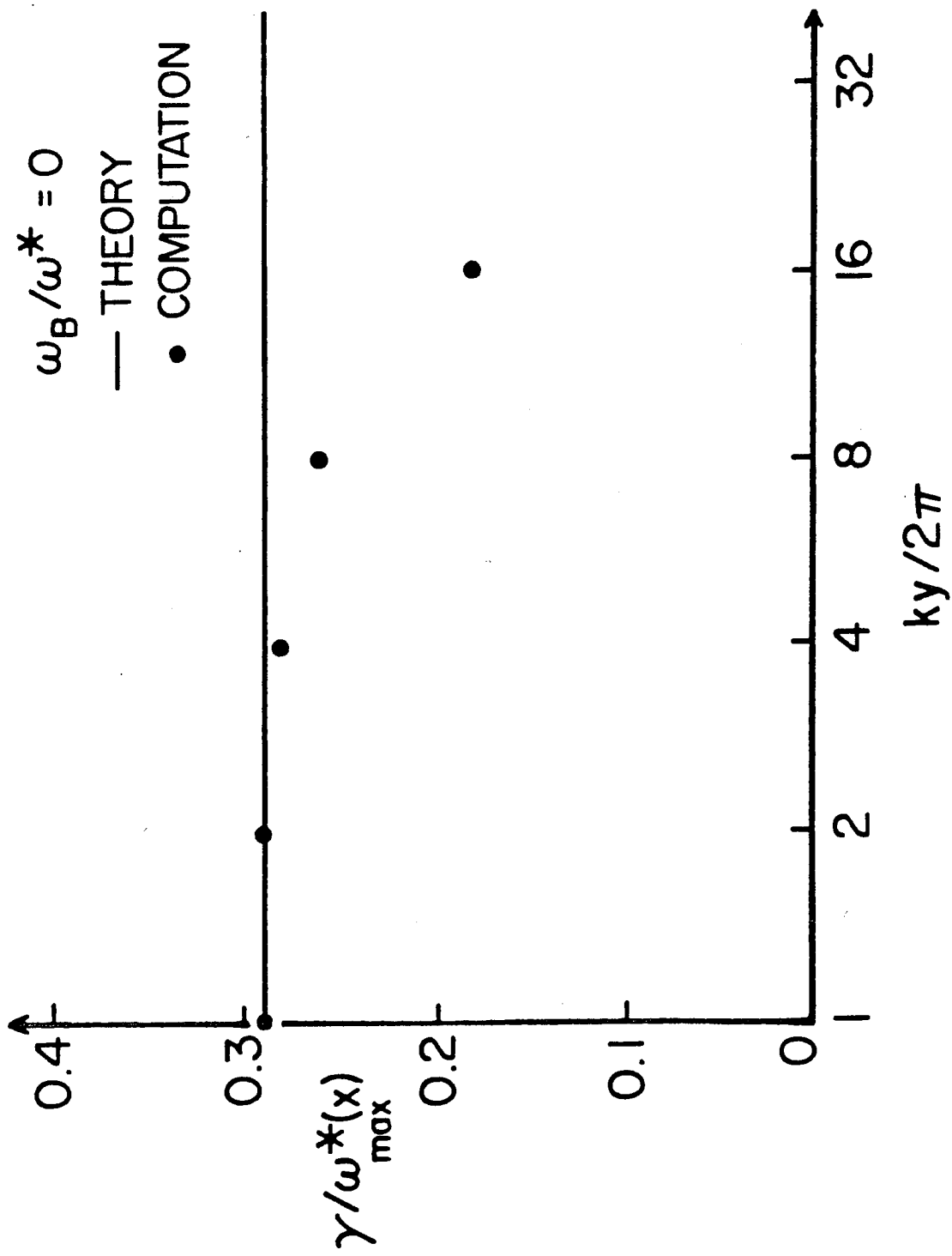
Fig. 1

Fig. 2

$\omega_B/\omega^* = 0$

— THEORY

• COMPUTATION

$\gamma/\omega^*_{max}(x)$

ky/2π

Fig. 3

Fig. 4

a)

$T_{min} = 1.0$ $T_{max} = 2.2$

b)

Fig. 5

a)

$B_{min} = 0.78$ $B_{max} = 1.3$

b)

Fig. 6

Fig. 7

a)

$T_{min} = 0.79$ $T_{max} = 2.6$

b)

Fig. 8

a)

$B_{min} = 0.52$ $B_{max} = 0.88$

b)

$<B>_y$
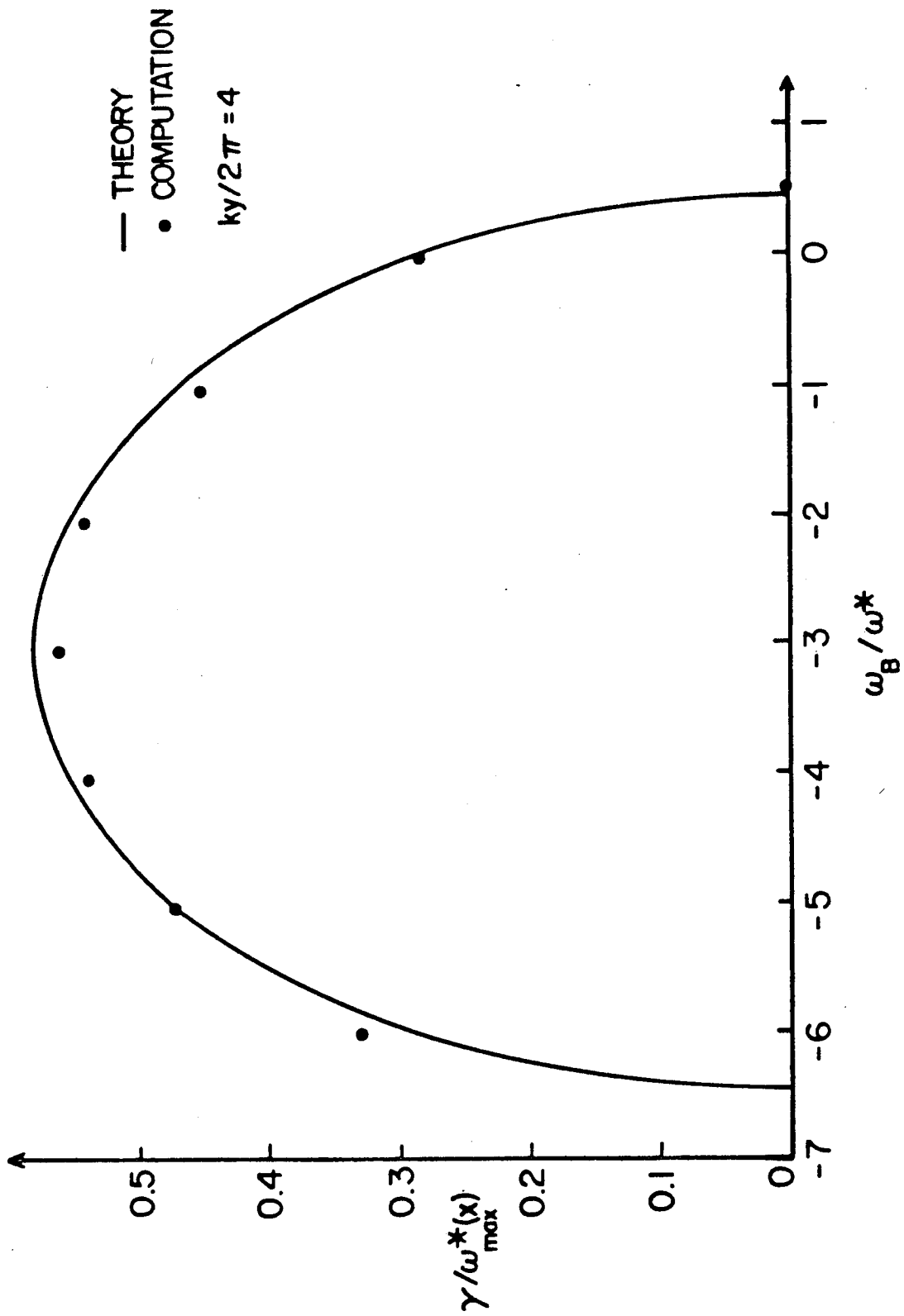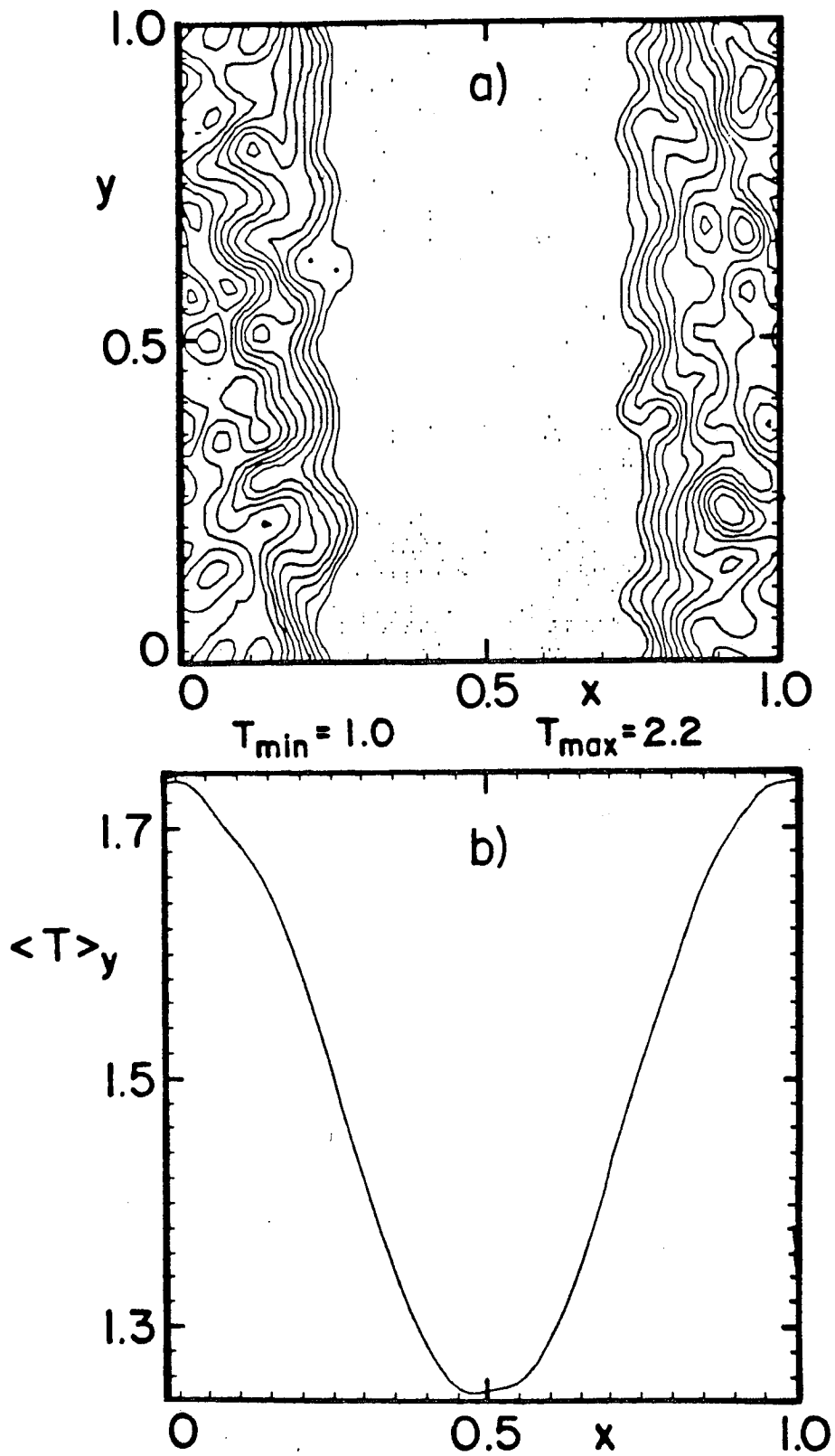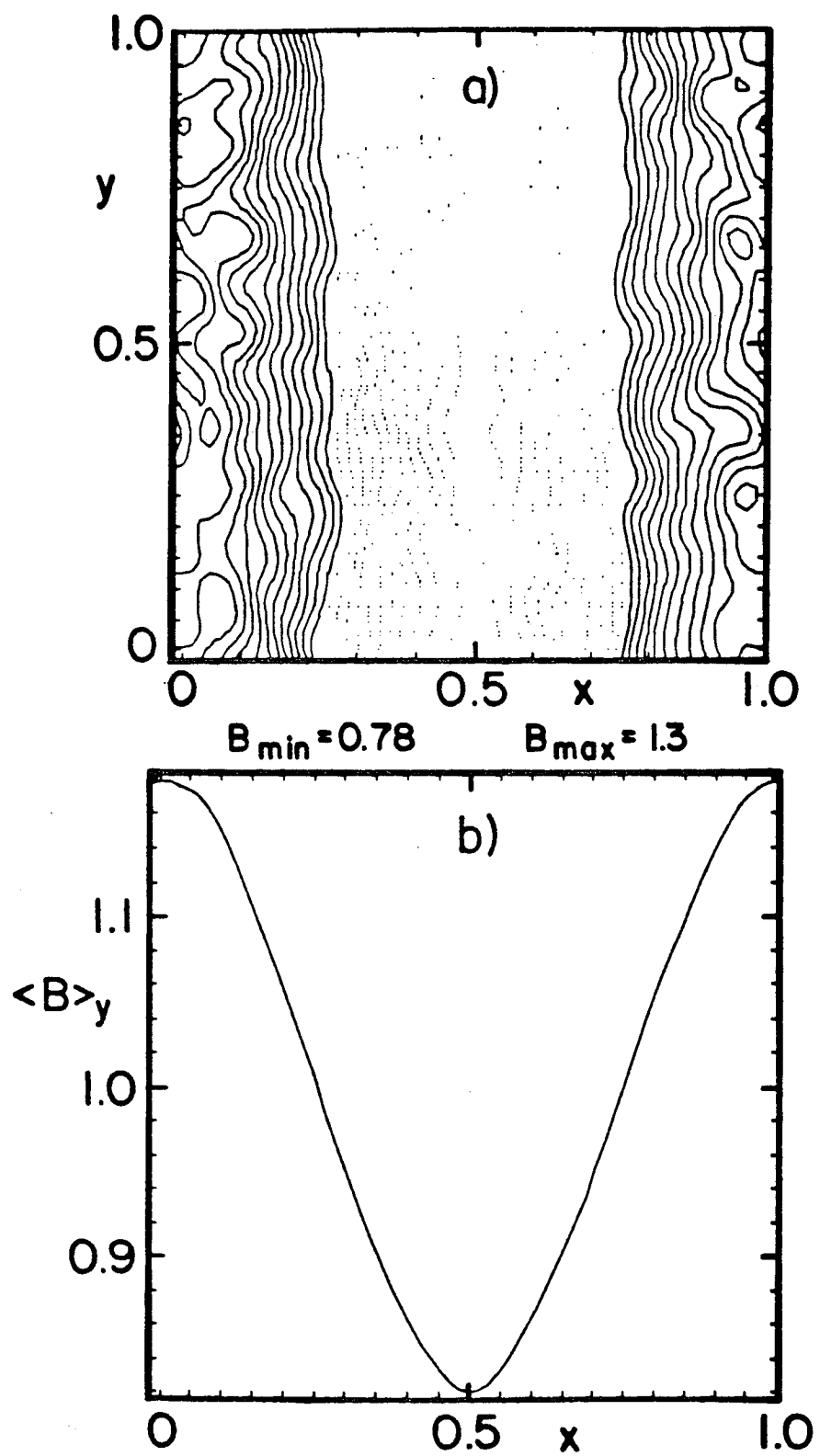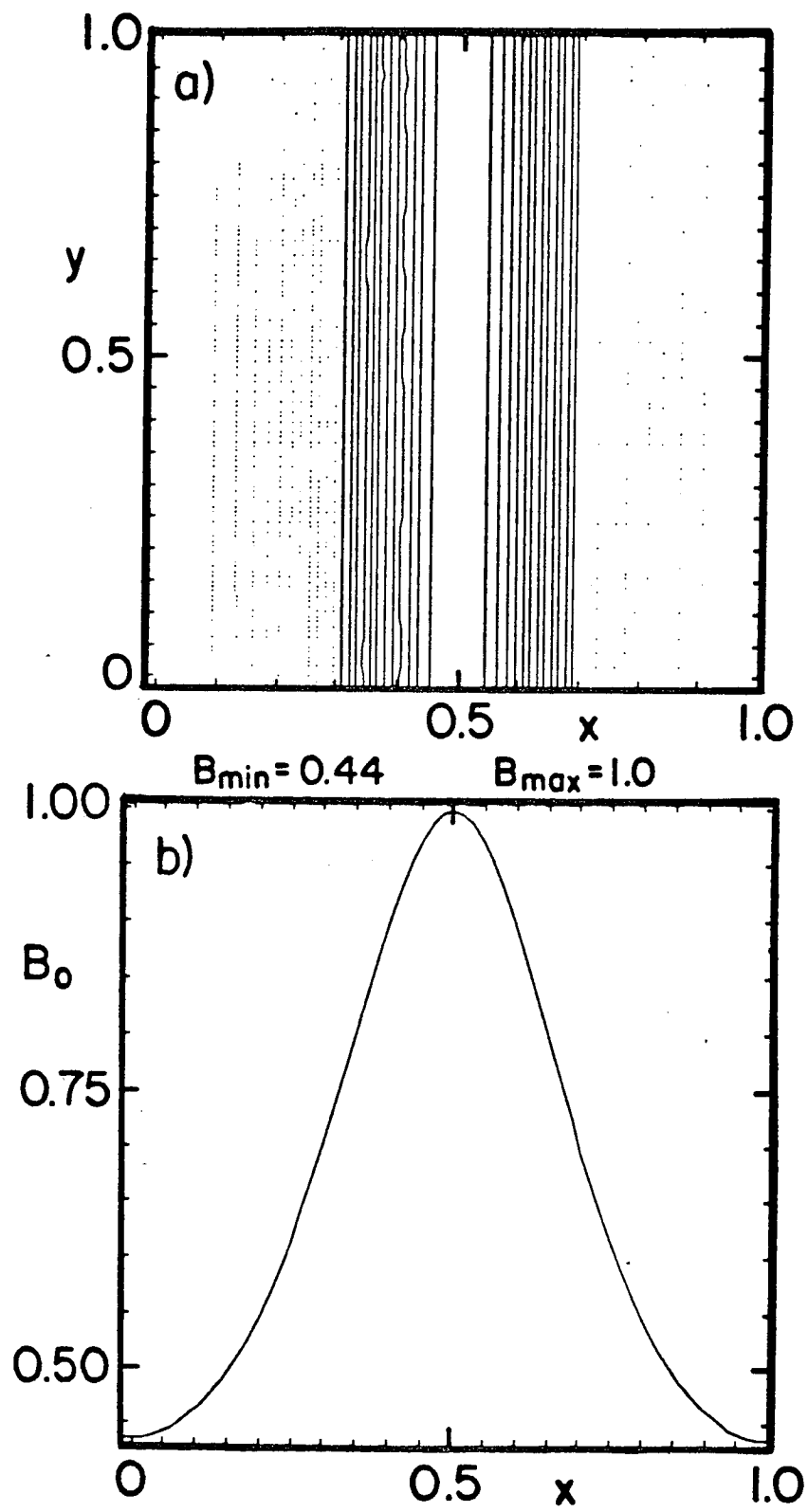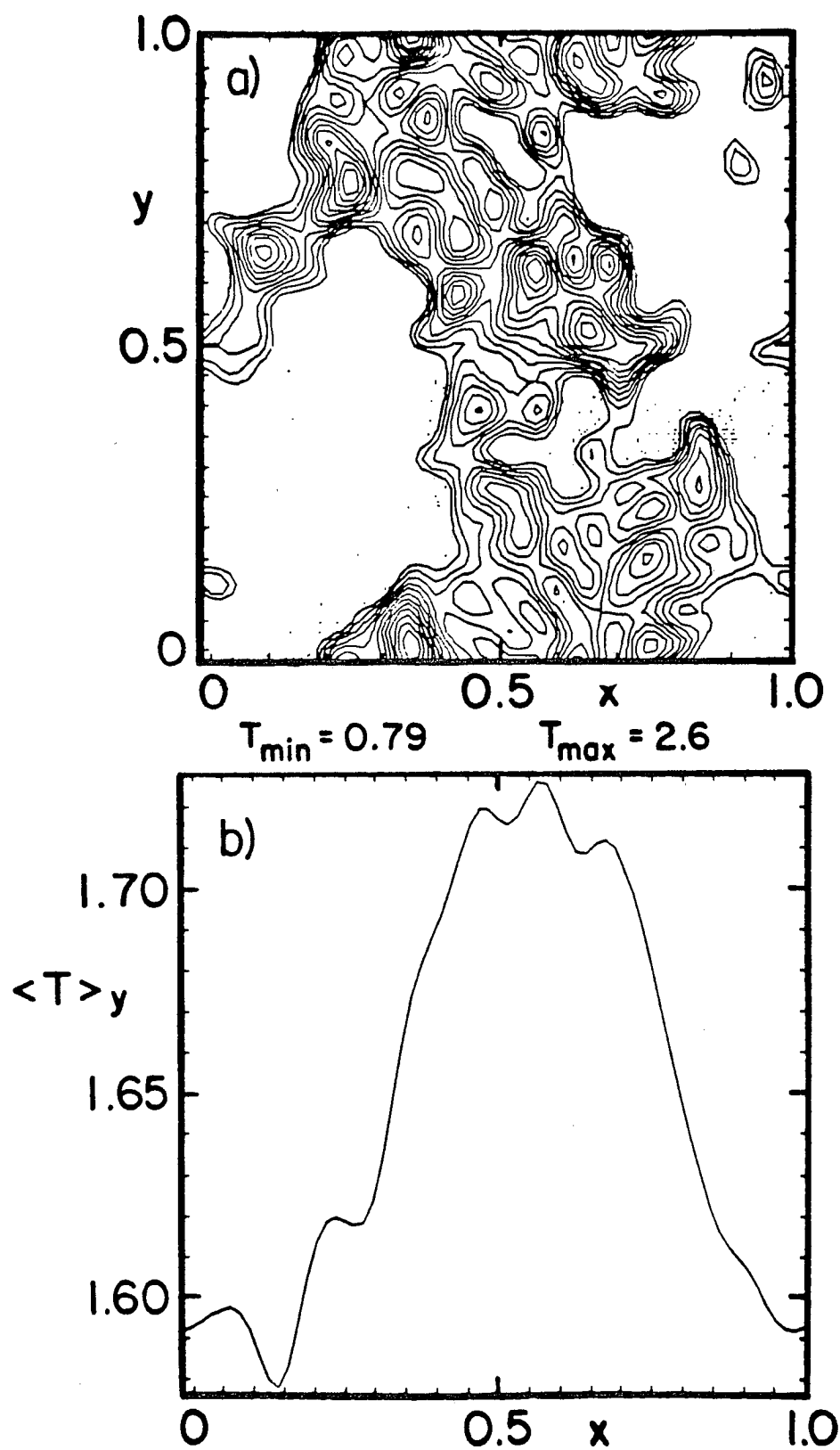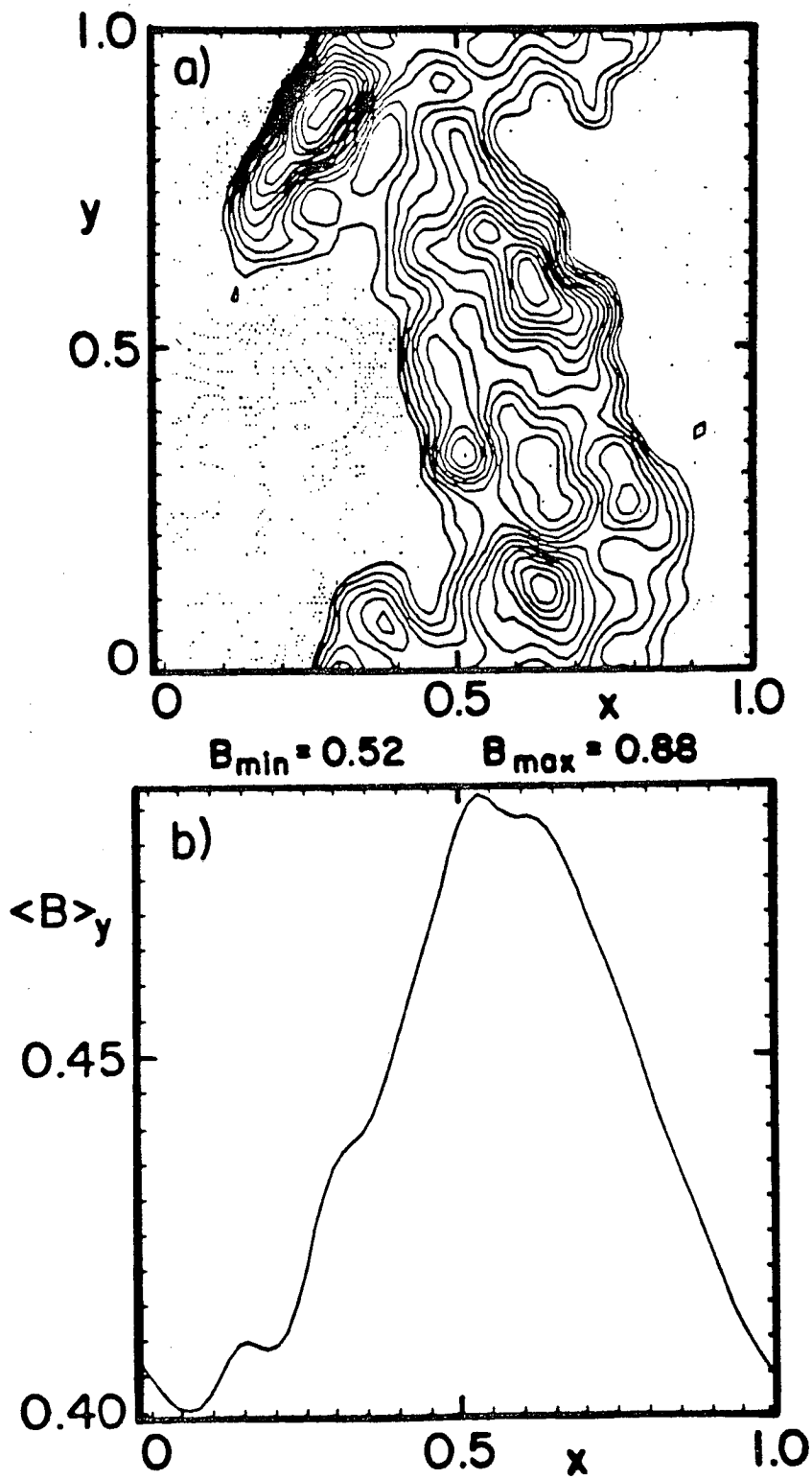
Fig. 9

Fig. 10

Fig. 11

Fig. 12

Fig. 13